JOURNAL OF THERMOPHYSICS AND HEAT TRANSFER
Vol. 20, No. 2, April–June 2006

Bridgman–Stockbarger Growth of Binary Alloyed Semiconductor Crystals with Steady Magnetic Fields

X. Wang* and N. Ma†
North Carolina State University, Raleigh, North Carolina 27695

Single crystals of alloyed compound semiconductor crystals such as gallium–aluminum–antimonide are needed for optoelectronic devices. These crystals are solidified from a solution of molten gallium–antimonide and aluminum–antimonide in a Bridgman–Stockbarger furnace. During the growth of alloyed semiconductor crystals, the solute's concentration is not small so that the density differences in the melt are very large. These compositional variations drive compositionally driven buoyant convection, or solutal convection, in addition to thermally driven buoyant convection. These buoyant convections drive convective species transport, which produce nonuniformities in the concentration in both the melt and the crystal. A numerical model is presented for the unsteady transport for the growth of alloyed semiconductor crystals during the vertical Bridgman–Stockbarger process with a steady axial magnetic field. Predictions of alloy concentration in the crystal and in the melt at several different stages during crystal growth are presented.

Nomenclature

a	=	dimensionless length of the ampoule
B	=	magnetic flux density
Bi	=	Biot number for the heat transfer from the furnace and through the ampoule wall
b	=	dimensionless depth of the melt
C	=	dimensionless concentration of the solute in the melt
C_s	=	dimensionless concentration in the crystal
C_0	=	initially uniform mole fraction of aluminum–antimonide in the melt
C^*	=	concentration or mole fraction of solute in the melt
c_p	=	specific heat of the melt
D	=	diffusion coefficient for the solute in the molten semiconductor
d	=	dimensionless distance between the crystal–melt interface and the vertical position in the furnace where the adiabatic and the hot zone meet
g	=	gravitational acceleration
Ha	=	Hartmann number
h	=	heat transfer coefficient between the outside surface of the melt and the furnace
$\boldsymbol{j}$	=	dimensionless electric current density
k	=	thermal conductivity of the melt
k_s	=	segregation coefficient for aluminum–antimonide in gallium–antimonide
N	=	interaction parameter
$\hat{\boldsymbol{n}}$	=	outward unit normal vector
Pe_g	=	growth Péclet number
Pe_m	=	species transport Péclet number
Pe_t	=	thermal Péclet number
p	=	dimensionless pressure
R	=	crystal radius or inner radius of ampoule
Re_m	=	magnetic Reynolds number
r	=	dimensionless radial coordinate in the melt
$\hat{\boldsymbol{r}}$	=	unit vector in the radial direction for the cylindrical coordinate system
T	=	dimensionless temperature in the melt
T_f	=	dimensionless furnace temperature
T_s	=	dimensionless solidification temperature at initial uniform concentration
T_s^*	=	solidification temperature
T^*	=	temperature in the melt
t	=	dimensionless time
U	=	characteristic velocity of the melt
U_g	=	growth rate or velocity of the crystal-melt interface
$\boldsymbol{v}$	=	dimensionless velocity in the melt
v_r	=	dimensionless radial velocity in the melt
v_z	=	dimensionless axial velocity in the melt
z	=	dimensionless axial coordinate in the melt
$\hat{\boldsymbol{z}}$	=	unit vector in the axial direction for the cylindrical coordinate system
β_C	=	compositional coefficient of volumetric expansion
β_T	=	thermal coefficient of volumetric expansion
Γ	=	difference between the melt concentration at the centerline and at the periphery at the crystal–melt interface
$(\Delta C)_0$	=	characteristic mole fraction variation
$(\Delta T)_0$	=	difference between the hot-zone temperature and the solidification temperature at the initial concentration
ζ	=	dimensionless rescaled axial coordinate in the melt
λ_C	=	buoyancy parameter
μ	=	dynamic viscosity of the melt
μ_p	=	magnetic permeability of the melt
ρ	=	density of the melt
ρ_0	=	density of the melt at the solidification temperature for pure gallium–antimonide
σ	=	electrical conductivity of the melt
ϕ	=	dimensionless electric potential
ψ	=	dimensionless Stokes stream function in the melt
ω	=	dimensionless growth rate or dimensionless velocity of the crystal–melt interface

Received 16 January 2005; revision received 9 May 2005; accepted for publication 27 May 2005.

*Graduate Research Assistant, Department of Mechanical and Aerospace Engineering, Campus Box 7910.

†Assistant Professor, Department of Mechanical and Aerospace Engineering, Campus Box 7910; nancy_ma@ncsu.edu. Senior Member AIAA.

I. Introduction

MANY optoelectronic devices are produced on wafers sliced from single crystals of alloyed compound semiconductor crystals, such as gallium–aluminum–antimonide (GaAlSb) and are grown by various methods such as the Bridgman–Stockbarger process, the vertical gradient freezing process, and the liquid-encapsulated Czochralski process. For the growth of a binary alloyed compound semiconductor crystal, the crystal is grown from a

solution of two molten compound semiconductors, and one component is generally rejected back into the melt. For example, GaAlSb is solidified from a solution of gallium–antimonide (GaSb) and aluminum–antimonide (AlSb). During growth, GaSb is rejected into the melt along the crystal–melt interface, which leads to a large concentration of GaSb near the growth interface. Anything that causes this elevated concentration to become nonuniform across the interface leads to compositional variations in the crystal, which is called radial segregation. Density differences caused by both compositional and thermal variations in the melt drive solutal and thermal convection, respectively, which lead to compositional variations both in the melt and in the crystal.

During crystal growth without a magnetic field or with a weak magnetic field, turbulent or oscillatory melt motions can produce undesirable spatial oscillations of the concentration, or microsegregation, in the crystal.[1] Turbulent or oscillatory melt motions lead to fluctuations in the heat transfer across the growth interface from the melt to the crystal. Because the local rate of crystallization depends on the balance between the local heat fluxes in the melt and the crystal, fluctuations in the heat flux from the melt create fluctuations in the local growth rate, which create microsegregation. A moderate magnetic field can be used to create a body force that provides an electromagnetic (EM) damping of the melt motion and to eliminate oscillations in the melt motion and, thus, in the concentration of the crystal. Unfortunately, the elimination of mixing and a moderate or strong EM damping of the residual melt motion may lead to a large variation of the crystal's composition in the direction perpendicular to the growth direction (radial macrosegregation).

On the other hand, if the magnetic field strength is so strong that the melt motion is reduced sufficiently so that it has no effect on the composition in the crystal, then this diffusion controlled species transport may produce a radially and axially uniform composition in the crystal grown. To achieve diffusion-controlled species transport, the species transport Péclet number $Pe_m = UR/D$ must be small, where U is the characteristic velocity for the magnetically damped melt motion and is inversely proportional to the square of the magnetic flux density B, whereas R is the characteristic dimension of the melt and D is the diffusion coefficient for the species in the molten semiconductor. If $Pe_m \ll 1$, then the characteristic ratio of convection to diffusion of species is small and the species transport is diffusion controlled. However, because typical values of D are extremely small,[2] that is, $1\text{–}2 \times 10^{-8}$ m^2/s, it would not be practical to grow a crystal in the extremely large field strength that would be required to achieve diffusion-controlled species transport. Even for crystal growth in microgravity, it is not possible to achieve diffusion-controlled species transport.[3] Therefore, the objective is to identify a magnetic field that is strong enough to eliminate flow oscillations but that moderately damps the melt motion to improve both radial and axial uniformity in the crystal. Watring and Lehoczky[4] have shown that the radial variations between the maximum and minimum concentrations can be decreased by more than a factor of three with the application of a 5-T magnetic field, arising because the magnetic field retards the sinking of the heavier melt to the center of the ampoule, which results in less radial segregation. Ramachandran and Watring[5] reported a reduction in the radial segregation in all of their samples that were grown in a magnetic field.

In a previous pair of studies,[6,7] we presented an asymptotic and numerical solution for the solutal convection during the solidification of an alloyed crystal in a rectangular container with axial[6] and transverse[7] magnetic fields. This approach treated growth for strong fields for which effects of inertia and convective heat transfer are negligible[8] and involved an analytic solution to the internal energy equation, a hybrid solution for the simplified Navier–Stokes and EM equations, and a numerical solution for the full species transport equation. This treatment is only valid for strong magnetic fields, and we treated a magnetic field strength of 2 T. Before these studies, Tagawa et al.,[9] Davoust et al.,[10] and Ma and Walker[11] performed asymptotic analysis on the melt motion in Bridgman-like geometries with strong magnetic fields. Talmage et al.[12] specifically studied the effects of inertia during doped growth in a strong magnetic field. The purpose of the present study is to treat numerically the full transient non-linear equations that are valid for any value of the magnetic field strength.

Garandet and Alboussière[13] reviewed the literature on experimental studies of Bridgman–Stockbarger growth of semiconductor crystals with magnetic fields, and Walker[14] reviewed the use of asymptotic methods in modeling of semiconductor crystal growth with strong magnetic fields.

II. Problem Formulation

This paper treats the unsteady, axisymmetric species transport of AlSb in a GaSb melt during the vertical Bridgman–Stockbarger process with an externally applied, uniform, steady, axial magnetic field $B\hat{z}$ Here, $\hat{r}$, $\hat{\theta}$, and $\hat{z}$ are the unit vectors for the cylindrical coordinate system. During the Bridgman–Stockbarger process, the ampoule is moved from an isothermal hot zone where the solution of GaSb and AlSb has been melted, through an adiabatic or thermal-gradient zone where the melt solidifies, and into a cold zone where the crystal is cooled. Our dimensionless problem is shown in Fig. 1. The coordinates and lengths are normalized by the ampoule's inner radius R, and a is the dimensionless length of the ampoule. The melt velocity $\boldsymbol{v}$ is normalized by the characteristic velocity for the magnetically damped buoyant convection,[15]

$$U = \rho g \beta_T (\Delta T)_0 \big/ \sigma B^2 \tag{1}$$

where $g = 9.81$ m^2/s, ρ is the melt's density at the solidification temperature T_s^*, β_T is the thermal volumetric expansion coefficient, σ is the melt's electrical conductivity, and $(\Delta T)_0$ is the difference between the hot-zone temperature and T_s^*. The crystal–melt interface moves at a constant velocity $U_g = \omega U$, where ω is the dimensionless interface velocity. The planar crystal–melt interface lies at $z = -b$, where the instantaneous axial length of the melt $b(t) = a - \omega t$ decreases during growth. With time t normalized by R/U, the dimensionless time to grow the entire crystal is a/ω.

The electric current in the melt produces an induced magnetic field, which is superimposed on the applied magnetic field produced by the external magnet. The characteristic ratio of the induced to the applied magnetic field strengths is the magnetic Reynolds number,

$$Re_m = \mu_p \sigma U R \tag{2}$$

where μ_p is the magnetic permeability of the melt. For all crystal-growth processes, $Re_m \ll 1$, and the additional magnetic fields produced by the electric currents in the melt are negligible.

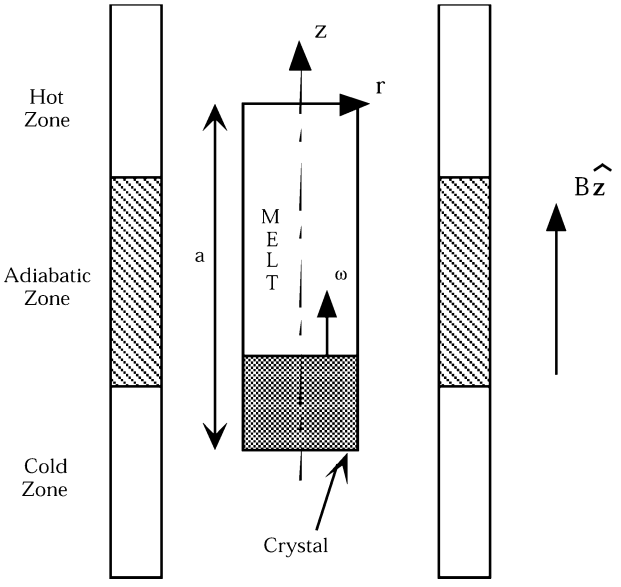

Fig. 1 Vertical Bridgman-Stockbarger ampoule with uniform, steady, axial magnetic field $B\hat{z}$ and with coordinates normalized by the ampoule's inner radius.

We assume that the temperature differences and compositional variations are sufficiently small that all of the thermophysical properties of the melt can be considered uniform and constant except for the density in the gravitational body force term of the momentum equation. In this Boussinesq-like approximation, the characteristic temperature difference $(\Delta T)_0$ and characteristic mole fraction difference $(\Delta C)_0$ are assumed to be sufficiently small that the melt's density is a linear function of temperature and composition, given by

$$\rho = \rho_0\left[1 - \beta_T\left(T^* - T_0\right) - \beta_C\left(C^* - C_0\right)\right] \tag{3}$$

and that $\beta_T(\Delta T)_0 \ll 1$ and $\beta_C(\Delta C)_0 \ll 1$, where ρ_0 is the density of the melt at the solidification temperature for pure GaSb, T^* is the temperature in the melt, C^* is the mole fraction of the solute (AlSb) in the melt, and C_0 is the initially uniform mole fraction in the melt before crystal growth begins. Here, β_T and β_C are the thermal and compositional coefficients of volumetric expansion, respectively.

When the Boussinesq approximation is used the equations governing the transport in the melt are

$$N^{-1}\left(\frac{\partial \boldsymbol{v}}{\partial t} + \boldsymbol{v}\cdot\nabla\boldsymbol{v}\right) = -\nabla p + [T + \lambda_c(C-1)]\hat{z} + \boldsymbol{j}\times\hat{z} + Ha^{-2}\nabla^2\boldsymbol{v} \tag{4a}$$

$$\nabla\cdot\boldsymbol{v} = 0 \tag{4b}$$

$$\nabla\cdot\boldsymbol{j} = 0 \tag{4c}$$

$$\boldsymbol{j} = -\nabla\phi + \boldsymbol{v}\times\hat{z} \tag{4d}$$

$$Pe_t\left(\frac{\partial T}{\partial t} + \boldsymbol{v}\cdot\nabla T\right) = \nabla^2 T \tag{4e}$$

$$\frac{\partial C}{\partial t} + \boldsymbol{v}\cdot\nabla C = Pe_m^{-1}\nabla^2 C \tag{4f}$$

where $\boldsymbol{v}(\boldsymbol{r}, \zeta, t) = v_r\hat{\boldsymbol{r}} + v_z\hat{\boldsymbol{z}}$ is the velocity of the melt normalized by U, p is the deviation of the pressure from the hydrostatic pressure normalized by $\sigma B^2 UR$, $\boldsymbol{j}$ is the electric current density normalized by σUB, ϕ is the electric potential function normalized by UBR, T is the deviation of the temperature from the hot-zone temperature normalized by the characteristic temperature difference in the melt $(\Delta T)_0$, and C is the mole fraction of AlSb in the GaSb melt normalized by the melt's initial uniform concentration C_0. The characteristic temperature difference in the melt is the difference between the hot-zone temperature and the melting temperature at concentration C_0. Here, R is the inner radius of the ampoule or the radius of the crystal. Also $\zeta = 1 + 2z/b$ is a rescaled axial coordinate so that $-1 \le \zeta \le +1$ for all time.

In the Navier–Stokes equation (4a), the interaction parameter $N = \sigma B^2 R/\rho U$ is the characteristic ratio of the EM body force to the inertial force in the melt, whereas the Hartmann number $Ha = BR(\sigma/\mu)^{1/2}$ is the square root of the characteristic ratio of the EM body force to the viscous force in the melt. In Eq. (4a), the buoyancy parameter is $\lambda_c = \beta_C C_0/\beta_T(\Delta T)_0$. In the energy equation (4e), the characteristic ratio of the convective to conductive heat transfer is the thermal Péclet number $Pe_t = \rho c_p UR/k$, where c_p is the melt's specific heat and k is the melt's thermal conductivity.

The no-slip and no-penetration conditions are applied along the surfaces of the ampoule. The radial and axial velocities along the crystal-melt interface are zero. The thermal boundary conditions at $\zeta = +1$, for $0 \le r \le 1$, is[16]

$$T = 0 \tag{5a}$$

and at $r = 1$, for $-1 \le \zeta \le +1$, is

$$\frac{\partial T}{\partial r} = Bi(T_f - T) \tag{5b}$$

where $T_f(\zeta)$ is the dimensionless furnace temperature, whereas the Biot number for the heat transfer from the furnace and through the ampoule wall is $Bi = hR/k$, where h is the heat transfer coefficient between the outside surface of the melt and the furnace. In the hot zone, $T_f = 0$ for $(-b + 2d)/b < \zeta < 1$, and in the thermal-gradient zone, $T_f = -1 + (\zeta + 1)b/(2d)$ for $-1 < \zeta(-b + 2d)/b$. Here, d is the dimensionless distance between the crystal–melt interface and the vertical position in the furnace where the adiabatic and the hot zone meet. Along the crystal-melt interface at $z = -b$, at $\zeta = -1$, for $0 \le r \le 1$,

$$T = T_s \tag{6}$$

where T_s is the dimensionless solidification temperature the deviation of the dimensional temperature T_s^* from the hot-zone temperature normalized by the characteristic temperature difference. Here,

$$T_s^*(C^*) = 710 + 855C^* - 1111C^{*2} + 1060C^{*3} - 450C^{*4} \tag{7}$$

where T_s^* is in degrees Celsius. Equation (7) is an estimation of the solidification temperature as a function of the mole fraction of AlSb in the melt, which is based on experimental data for the liquidus curve in the pseudobinary phase diagram for GaAlSb.[17]

At the beginning of crystal growth, the melt concentration, normalized by the initial uniform concentration, is $C(r, z, t = 0) = 1$. The initial condition for the temperature and velocity is given by the steady-state solution to Eqs. (4a–4e), that is, without the time derivatives in Eqs. (4a) and (4e). We apply the no-slip and no-penetration conditions for the velocity along the surfaces of the ampoule. We apply the thermal boundary conditions (5a) and (5b) along $\zeta = +1$ and $r = 1$, respectively. Along $\zeta = -1$, we apply the condition $T = -1$. We use a Chebyshev spectral collocation method with Gauss–Lobatto collocation points in r and ζ. Because Eqs. (4a) and (4e) are nonlinear, we use a Newton–Raphson iterative method. We define the stream function ψ,

$$v_r = \frac{1}{r}\frac{\partial\psi}{\partial z} \tag{8a}$$

$$v_z = -\frac{1}{r}\frac{\partial\psi}{\partial r} \tag{8b}$$

In Figs. 2a and 2b, we present the initial temperature and stream function, respectively, with $a = 1$ and $d = 0.1$ and with $B = 0.1$ T for which $N = 2.196$, $Ha = 15.60$, and $Pe_t = 4.914$. In Fig. 2a, the heat transfer is dominated by conduction and the thermal gradients are concentrated in the region adjacent to the bottom of the ampoule because this region is adjacent to the furnace's thermal-gradient zone. In Fig. 2b, the hot fluid rises adjacent to the ampoule's periphery, flows radially inward along the top of the ampoule, flows axially downward along the centerline, and flows radially outward

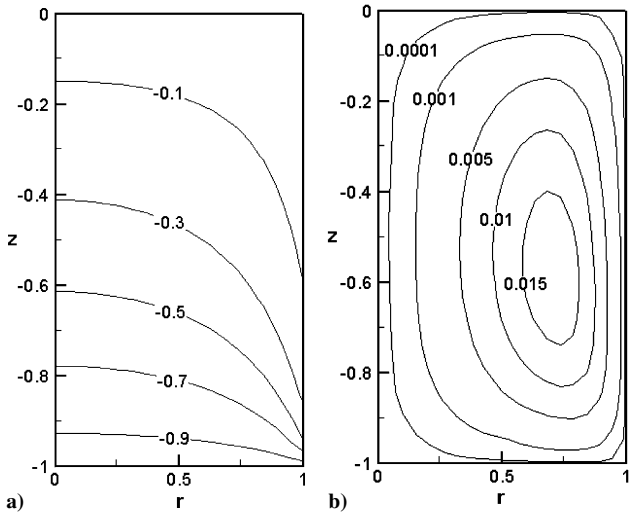

Fig. 2 Initial temperature and stream function for $B = 0.1$ T, $Bi = 10$, $a = 1$, and $d = 0.1$: a) $T(r, z, t = 0)$ and b) ψ $(r, z, t = 0)$.

along the bottom of the ampoule. Initially, the maximum value of the stream function is 0.01798.

The boundary conditions along the walls of the ampoule are $\hat{\boldsymbol{n}} \cdot \nabla C = 0$ where $\hat{\boldsymbol{n}}$ is the outward unit normal vector. Along the crystal–melt interface, at $\zeta = -1$, for $0 \le r \le 1$,

$$\frac{2}{b}\frac{\partial C}{\partial \zeta} = Pe_g(k_s - 1)C \tag{9}$$

where $Pe_g = U_g R/D = \omega Pe_m$ is the growth Péclet number. In Eq. (9), k_s is the segregation or distribution coefficient for AlSb in the GaSb melt. The rejection of GaSb along the crystal–melt interface creates a GaSb-rich region in which GaSb diffuses away from the interface. A curve fit based on the experimental data presented by Osamura et al.[17] gives a relationship for $k_s(C^*)$,

$$k_s(C^*) = 7.3 - 53.9C^* + 253.7C^{*2} - 672.3C^{*3} + 979.45C^{*4} - 727.88C^{*5} + 214.7C^{*6} \tag{10}$$

The value of k_s decreases as the mole fraction of AlSb increases.

We used a Chebyshev spectral collocation method to solve Eqs. (4a–4f) with Gauss–Lobatto collocation points in r and ζ. We used a sufficient number of collocation points to resolve the velocity and concentration gradients. For the time derivatives in Eqs. (4a), (4e), and (4f), we used a second-order implicit time integration scheme to integrate from $t = 0$ to a time that is slightly less than a/ω. We chose a large enough number of time steps so that the results are not changed by increasing the number of time steps. For example, with $a = 1$, $d = 0.1$, and $U_g = 23$ μm/s and with $B = 0.1$ T and $C_0 = 0.001$, for which $N = 2.196$, $Ha = 15.60$, $Pe_t = 4.914$, $Pe_m = 2124.4$, $Pe_g = 8.625$, $\lambda_C = 0.2267$, $\omega = 0.00406$, and the time to grow a crystal is $a/\omega = 246.3$, we used 61 and 41 collocation points in the radial and axial directions, respectively, and 4800 time steps. When we doubled the number of collocation points in the radial direction, the maximum value of the stream function changed by 0.01%, and the maximum value of the melt concentration changed by 0.0001% when $t = 0.05131$. When we doubled the number of collocation points in the axial direction, the maximum value of the stream function changed by 0.008%, and the maximum value of the melt concentration changed by 0.0001% when $t = 0.05131$. When we doubled the number of time steps, the maximum value of the stream function changed by 0.0056%, and the maximum value of the melt concentration changed by 0.001% when $t = 0.05131$.

When it is assumed that there is no diffusion of species in the solid crystal, the solute distribution in the crystal, $C_s(r, z)$, normalized by the initial uniform solute concentration in the melt, is given by

$$C_s(\boldsymbol{r}, z) = k_s C(\boldsymbol{r}, \zeta = -1, t = z/\omega) \tag{11}$$

Unfortunately, the axial segregation is unavoidable in the current system because the ampoule is closed and the segregation coefficient k_s is not equal to one.[18] However, recent research has shown that it is possible to produce a crystal that has a significant axial length that is axially uniform.[19] This can be accomplished by continuously replenishing the melt throughout growth with fluid that has a composition chosen to offset the rejection of species along the crystal–melt interface.[20]

III. Results

For our typical Bridgman crystal growth process with the thermophysical properties of GaAlSb and with $a = 1$ and $d = 0.1$, $U = 0.00005665B^{-2}$ m/s, $N = 21955.4B^4$, $Ha = 156.05B$, $Pe_t = 0.04914B^{-2}$, $Pe_m = 21.24B^{-2}$, $Pe_g = 0.375U_g$, $\lambda_C = 226.5C_0$, $\omega = 0.01765U_g B^2$, and $a/\omega = 56.66U_g^{-1}B^{-2}$ with U_g in micrometers per second and B in tesla. We present results for $B = 0.1$ T and $U_g = 23$ μm/s, for which $U = 0.005665$ m/s, $N = 2.196$, $Ha = 15.60$, $Pe_t = 4.914$, $Pe_m = 2124.4$, $Pe_g = 8.625$, $\omega = 0.00406$, and the dimensionless time to grow a crystal is $a/\omega = 246.3$. We present results for several cases to investigate the effects of the initial uniform concentration C_0.

We begin by presenting results for $C_0 = 0.001$, for which $\lambda_C = 0.2267$. Figure 3 shows the contours of the melt concentration

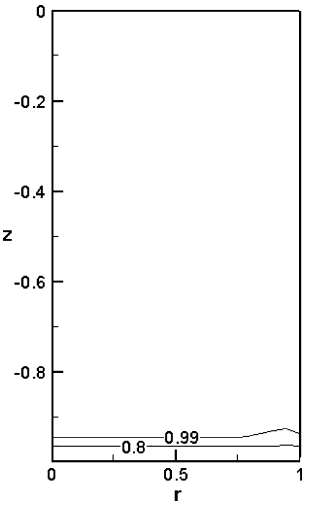

Fig. 3 Concentration in melt C $(r, z, t = 0.6158)$ for $B = 0.1$ T and $C_0 = 0.001$.

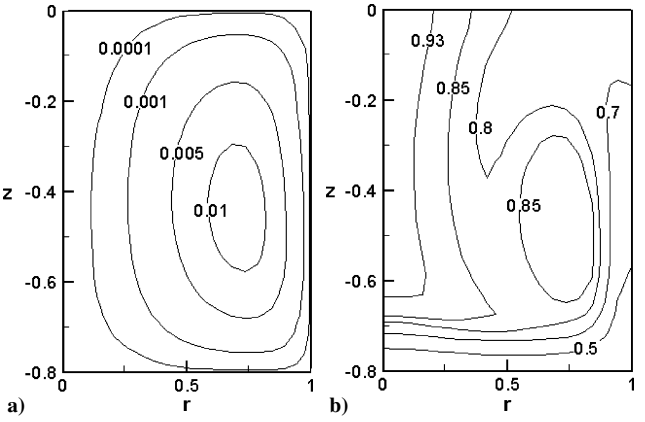

Fig. 4 Stream function in melt ψ (r, z, t) and concentration in melt C (r, z, t) for $B = 0.1$ T and $C_0 = 0.001$: a) ψ $(r, z, t = 49.26)$ and b) C $(r, z, t = 49.26)$.

C when 0.25% of the crystal has grown at $t = 0.6158$. Once crystal growth begins, the crystal absorbs AlSb and GaSb is rejected along the crystal–melt interface. Therefore, we refer to the melt adjacent to the interface as AlSb-depleted or GaSb-rich. At this time, the minimum value of the temperature is -1.0455, and the isotherms resemble those in Fig. 2a because the heat transfer is dominated by conduction for this small value of Péclet number Pe_t. With thermal convection alone, the melt flows axially upward along the periphery of the ampoule, flows radially inward along the top of the ampoule, flows axially downward along the centerline of the ampoule, and flows radially outward along the crystal–melt interface. The circulation due to thermal convection is counterclockwise. In Fig. 3 at a given axial position, the concentration near the centerline is higher than the concentration near the periphery. Because AlSb is lighter than GaSb, the melt near the centerline is lighter than the melt near the periphery. Therefore, the melt's compositional variations drive a weak circulation due to solutal convection that is clockwise and that opposes the circulation due to thermal convection. The contours of the stream function resemble those in Fig. 2b, but the maximum value of the stream function has decreased to 0.01794. In Fig. 3, the minimum value of the concentration is 0.4539, and most of the melt is at the initial uniform concentration $C = 1$. The species transport is dominated by diffusion as reflected in the contours of the concentration in Fig. 3, which are flat except near the periphery where there is a bump in the contour because the axially upward flow has convected the AlSb-depleted melt axially upward. For this stage of growth, the difference between the melt concentration at the centerline and at the periphery at the crystal–melt interface is $\Gamma = 0.002517$.

For $C_0 = 0.001$, we show the stream function ψ and concentration C in the melt at $t = 49.2641$ when 20% of the crystal has grown in Figs. 4a and 4b, respectively. In Fig. 4a, the maximum value of the

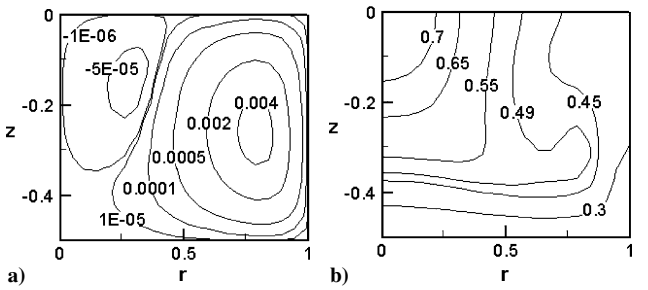

Fig. 5 Stream function in melt ψ (r, z, t) and concentration in melt C (r, z, t) for $B = 0.1$ T and $C_0 = 0.001$: a) $\psi(r, z, t = 123.15)$ and b) $C(r, z, t = 123.15)$.

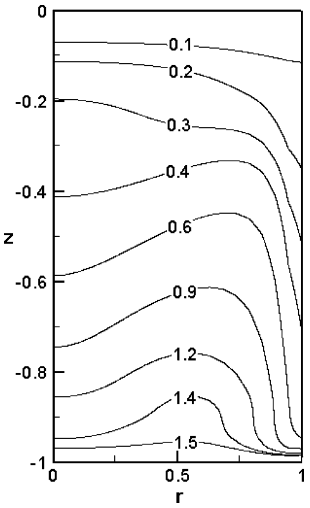

Fig. 6 Concentration in crystal C_s (r, z) for $B = 0.1$ T, $a = 1$, and $C_0 = 0.001$.

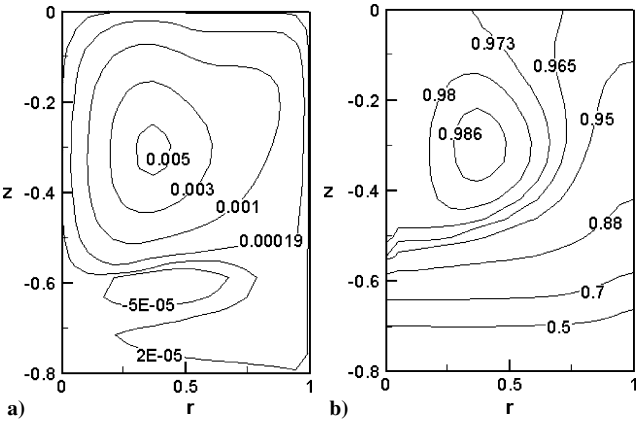

Fig. 7 Stream function in melt ψ (r, z, t) and concentration in melt C (r, z, t) for $B = 0.1$ T and $C_0 = 0.10$: a) ψ $(r, z, t = 49.26)$ and b) C $(r, z, t = 49.26)$.

stream function has further decreased to 0.01235. In Fig. 4b, the minimum and maximum values of the melt concentration are 0.04266 and 0.9775, respectively. The minimum value of the melt concentration is decreased significantly because the segregation coefficient is very large for AlSb in GaSb with $C_0 = 0.001$. The convection of species is strong enough that there is a closed contour with $C = 0.85$ in Fig. 4b. For this stage of growth, the difference between the melt concentration at the centerline and at the periphery at the crystal–melt interface is $\Gamma = 0.07936$. Figures 5a and 5b show the stream function ψ and concentration C in the melt at $t = 123.15$ when 50% of the crystal has grown. In Fig. 5a, the minimum and maximum values of the stream function are -0.00007516 and 0.004699, respectively. At this stage of growth, although the radial concentration difference has decreased compared with the earlier stage of growth presented in Fig. 4b, the thermal convection has also decreased because the melt depth has decreased. The relative importance of the solutal convection has increased and caused part of the flow to reverse direction as reflected in the clockwise circulation near $r = 0$ and $z = 0$ in Fig. 5a. In Fig. 5b, the minimum and maximum values of the melt concentration are further decreased to 0.04007 and 0.7420, respectively. For this stage of growth, the difference between the melt concentration at the centerline and at the periphery at the crystal–melt interface is $\Gamma = 0.02619$. Except for very early stages of growth, this difference has continuously decreased throughout growth. This is due to a combination of two factors. The average melt concentration decreases as growth progresses due to the absorption of AlSb along the crystal–melt interface and the transport of species along the crystal–melt interface reduces the segregation along the crystal–melt interface. For the remainder of growth, the shapes of the contours of stream function and melt concentration resemble those in Fig. 5a and 5b. The average melt concentration continues to decrease as the crystal–melt interface absorbs AlSb continuously throughout the growth. Near the end of the growth, the melt is left totally depleted of AlSb because the segregation coefficient is very large.

For $C_0 = 0.001$, we show the contours of the composition in the crystal in Fig. 6. The bottom of the crystal solidified with a relatively radially uniform composition because the AlSb-depleted melt did not have enough time to be convected away from the interface. As growth progresses, the contours of the concentration become more curved because the axially upward flow near $r = 1$ convects the AlSb-depleted melt axially upward and away from the interface. Near the end of growth, the average concentration in the melt is small due to the absorption along the interface. In addition, the compositional variations in the melt are small compared with earlier stages of growth so that the crystal is relatively radially uniform near $z = 0$. The axial composition in the crystal decreases as z increases.

To investigate the effects of the solutal convection, we increase the value of the initial uniform concentration to $C_0 = 0.10$ for which $\lambda_C = 22.67$. When 0.25% of the crystal has grown at $t = 0.6158$, the maximum value of the stream function is 0.02681, and the minimum value of the melt concentration is 0.5956. For this early stage of growth, the contours for the stream function and the concentration resemble those in Figs. 2b and 3, respectively. We show the stream function and concentration in the melt when 20% of the crystal has grown at $t = 49.26$ in Figs. 7a and 7b, respectively. In Fig. 7a, the minimum and maximum values of the stream function are -0.0001497 and 0.005414, respectively. Most of the melt circulates in the counterclockwise direction. The concentration gradient has become large enough so that the solutal convection has caused the flow to reverse so that there is a weak circulation in the clockwise direction near the crystal–melt interface as reflected in the $\psi = -0.00005$ contour in Fig. 7a. The counterclockwise circulation above is roughly 10 times stronger than the clockwise circulation below. In Fig. 7b, the minimum and maximum values of the concentration are 0.06609 and 0.9890, respectively. For this stage of growth, the species transport in the lower-half of the melt is mostly driven by diffusion. The convective species transport in the upper-half of the melt is much stronger, as reflected in the closed constant-concentration curves for $C = 0.98$ and $C = 0.986$ in Fig. 7b. For this stage of growth at $t = 49.26$, the difference between the melt concentration at the centerline and at the periphery at the crystal–melt interface is $\Gamma = 0.02600$. As growth progresses, the AlSb-depleted melt is convected axially upward, and the clockwise circulation due to the solutal convection moves axially upward as well. By the time 50% of the crystal has grown at $t = 123.15$, the clockwise circulation has moved to the upper-half of the melt as shown in the contours of the stream function presented in Fig. 8a. In Fig. 8a, the minimum and maximum values of the stream function are -0.0001855 and 0.0002409, respectively. At this time, the radial concentration gradient is larger in the upper volume of the melt than in the lower volume of the melt, as reflected in the constant-concentration curves presented in Fig. 8b. In Fig. 8b, the species transport is mostly driven by diffusion, and the minimum and maximum values of the concentration are 0.04443 and 0.9230, respectively. At this time, the

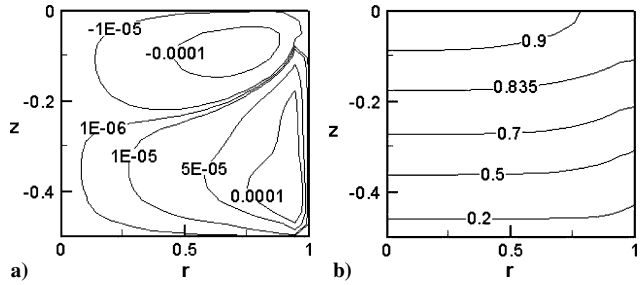

Fig. 8 Stream function in melt ψ (r, z, t) and concentration in melt C (r, z, t) for $B = 0.1$ T and $C_0 = 0.10$: a) ψ $(r, z, t = 123.15)$ and b) C $(r, z, t = 123.15)$.

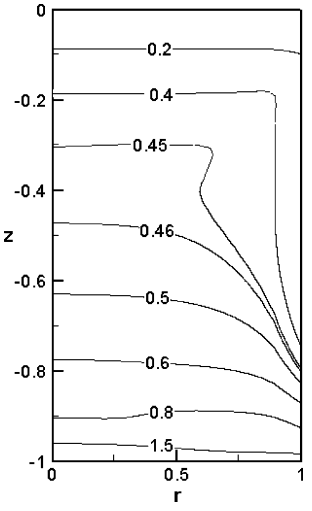

Fig. 9 Concentration in crystal C_s (r, z) for $B = 0.1$ T and $C_0 = 0.10$.

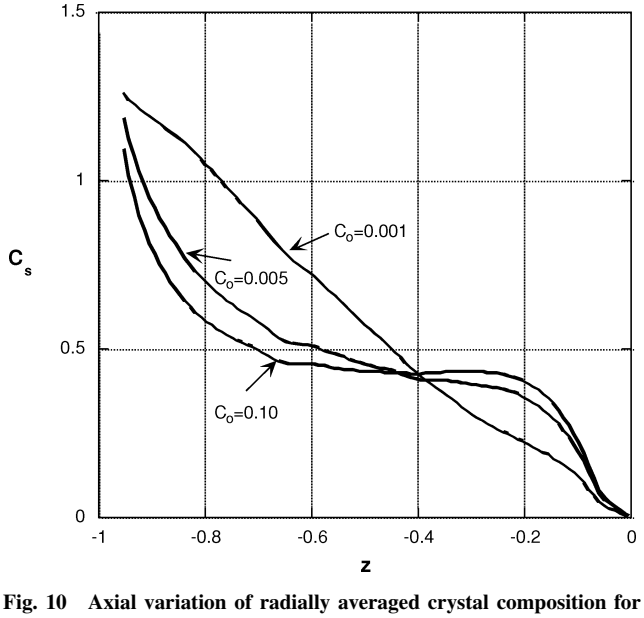

Fig. 10 Axial variation of radially averaged crystal composition for $C_0 = 0.001$, $C_0 = 0.005$, and $C_0 = 0.10$.

difference between the melt concentration at the centerline and at the periphery at the crystal–melt interface is $\Gamma = 0.02229$. For a given stage of growth, Γ for the current initial composition $C_0 = 0.10$ is smaller than the Γ for $C_0 = 0.001$. In Fig. 9, we show the constant-concentration curves in the crystal.

We show the axial variation of the radially averaged crystal concentration for $C_0 = 0.001$, $C_0 = 0.005$, and $C_0 = 0.10$ in Fig. 10. The segregation coefficient is very large as reflected by Eq. (10) so that the initial concentration in the crystal is very large. To see the details of the axial segregation, we have not included the data corresponding to values near $z = -1$ in Fig. 10 because these values are much larger than the values in the remainder of the crystal. Of course, the composition in the crystal decreases with z because $k_s > 1$. Moreover, because k_s is large, there is virtually no AlSb remaining in the melt at the end of growth so that the crystal concentration approaches zero as z approaches zero for all cases. As C_0 increases, the bulk of the crystal becomes more axially uniform as reflected in the flattening out of the curves.

IV. Conclusions

We have developed a numerical model that can accurately predict the unsteady transport in the melt and the species distribution in an alloyed crystal grown in a steady magnetic field. During vertical Bridgman–Stockbarger crystal growth with an axial magnetic field, the solutal convection opposes the thermal convection. When the initial uniform concentration C_0 increases, the relative importance of the solutal convection increases compared with the thermal convection, and the radial and axial uniformity of the crystal increases.

Acknowledgments

This research was supported by the U.S. Air Force Office of Scientific Research under Grant FA9550-04-1-0249. The calculations were performed on the Cray X1 and the SGI Origin 3000 Complex provided by the Department of Defense High Performance Computing Modernization Program under Grant AFSNH2487 and on the IBM pSeries 690 provided by the National Computational Science Alliance under Grant DMR030015.

References

[1]Walker, J. S., Henry, D., and BenHadid, H., "Magnetic Stabilization of the Buoyant Convection in the Liquid-Encapsulated Czochralski Process," *Journal of Crystal Growth*, Vol. 243, No. 1, 2002, pp. 108–116.

[2]Khine, Y. Y., Banish, R. M., and Alexander, J. I. D., "Convective Effects During Diffusivity Measurements in Liquids with an Applied Magnetic Field," *International Journal of Thermophysics*, Vol. 23, No. 3, 2002, pp. 649–666.

[3]Ma, N., and Walker, J. S., "Magnetic Damping of Buoyant Convection During Semiconductor Crystal Growth in Microgravity. Continuous Random g-gitters," *Physics of Fluids*, Vol. 8, No. 1/4, 1996, pp. 944–953.

[4]Watring, D. A., and Lehoczky, S. L., "Magneto-hydrodynamic Damping of Convection During Vertical Bridgman–Stockbarger Growth of HgCdTe," *Journal of Crystal Growth*, Vol. 167, No. 3/4, 1996, pp. 478–487.

[5]Ramachandran, N., and Watring, D. A., "Convection Damping by an Axial Magnetic Field During the Growth of HgCdTe by Vertical Bridgman Method—Thermal Effects," AIAA Paper 97-0450, Jan. 1997.

[6]Ma, N., "Solutal Convection During Growth of Alloyed Semiconductor Crystals in a Magnetic Field," *Journal of Thermophysics and Heat Transfer*, Vol. 17, No. 1, 2003, pp. 77–81.

[7]Wang, X., and Ma, N., "Strong Magnetic Field Asymptotic Model for Binary Alloyed Semiconductor Crystal Growth," *Journal of Thermophysics and Heat Transfer*, Vol. 18, No. 4, 2004, pp. 476–480.

[8]Ma, N., and Walker, J. S., "Inertia and Thermal Convection During Crystal Growth with a Magnetic Field," *Journal of Thermophysics and Heat Transfer*, Vol. 15, No. 1, 2001, pp. 50–54.

[9]Tagawa, T., Authie, G., and Moreau, R., "Buoyant Flow in Long Vertical Enclosures in the Presence of a Strong Horizontal Magnetic Field. Part 1. Fully-established Flow," *European Journal of Mechanics B—Fluids*, Vol. 21, No. 4, 2002, pp. 383–398.

[10]Davoust, L., Moreau, R., Cowley, M. D., Tanguy, P. A., and Bertrand, F., "Numerical and Analytical Modeling of the MHD Buoyancy-driven Flow in a Bridgman Crystal Growth Configuration," *Journal of Crystal Growth*, Vol. 180, No. 3/4, 1997, pp. 422–432.

[11]Ma, N., and Walker, J. S., "Liquid-metal Buoyant Convection in a Vertical Cylinder with a Strong Vertical Magnetic Field and with a Non-axisymmetric Temperature," *Physics of Fluids*, Vol. 7, No. 8, 1995, pp. 2061–2071.

[12]Talmage, G., Shyu, S. H., Moeny, M. J., Tavener, S., and Cliffe, K. A., "Inertial Effects on Electrically Conducting Fluids in the Presence of Transverse Magnetic Fields: An Example Problem," *International Journal of Engineering Science*, Vol. 36, No. 1, 1998, pp. 1–13.

[13]Garandet, J. P., and Alboussière, T., "Bridgman Growth: Modelling and Experiments," *The Role of Magnetic Fields in Crystal Growth*, Progress in Crystal Growth and Characterization of Materials, Vol. 38, edited by K. W. Benz, Elsevier, Oxford, 1999, pp. 73–132.

[14]Walker, J. S., "Models of Melt Motion, Heat Transfer, and Mass Transport During Crystal Growth with Strong Magnetic Fields," *The Role of Magnetic Fields in Crystal Growth*, Progress in Crystal Growth and Characterization of Materials, Vol. 38, edited by K. W. Benz, Elsevier, Oxford, 1999, pp. 195–213.

[15]Hjellming, L. N., and Walker, J. S., "Melt Motion in a Czochralski Puller with an Axial Magnetic Field: Motion due to Buoyancy and Thermocapillarity," *Journal of Fluid Mechanics*, Vol. 182, 1987, pp. 335–368.

[16]Ma, N., and Walker, J. S., "A Model of Dopant Transport During Bridgman Crystal Growth with Magnetically Damped Buoyant Convection," *Journal of Heat Transfer*, Vol. 208, No. 1, 2000, pp. 757–771.

[17]Osamura, K., Nakajima, K., and Murakami, Y., "Experiments and Calculation of the Al–Ga–Sb Ternary Phase Diagram," *Journal of the Electrochemical Society*, Vol. 126, No. 11, 1979, pp. 1992–1997.

[18]Wang, X., Ma, N., Bliss, D. F., and Iseler, G. W., "Semiconductor Crystal Growth by Modified Vertical Gradient Freezing with Electromagnetic Stirring," *Journal of Thermophysics and Heat Transfer*, Vol. 19, No. 1, 2005, pp. 95–100.

[19]Ma, N., Bliss, D. F., and Iseler, G. W., "Vertical Gradient Freezing of Doped Gallium–antimonide Semiconductor Crystals Using Submerged Heater Growth and Electromagnetic Stirring," *Journal of Crystal Growth*, Vol. 259, No. 1/2, 2003, pp. 26–35.

[20]Ma, N., Bliss, D. F., and Iseler, G. W., "Vertical Gradient Freezing of Doped Gallium–antimonide Semiconductor Crystals Using Submerged Heater Growth and Electromagnetic Stirring," *Journal of Crystal Growth*, Vol. 259, No. 1/2, 2003, pp. 26–35.